



LAWRENCE  
LIVERMORE  
NATIONAL  
LABORATORY

# Detection and Classification of Off-Normal Images During Automatic Alignment of High Energy Laser Beams

J. V. Candy, W. A. McClay, A. A. S. Awwal, S. W.  
Ferguson, S. C. Burkhart

March 21, 2005

Journal of Optical Society of America

## **Disclaimer**

---

This document was prepared as an account of work sponsored by an agency of the United States Government. Neither the United States Government nor the University of California nor any of their employees, makes any warranty, express or implied, or assumes any legal liability or responsibility for the accuracy, completeness, or usefulness of any information, apparatus, product, or process disclosed, or represents that its use would not infringe privately owned rights. Reference herein to any specific commercial product, process, or service by trade name, trademark, manufacturer, or otherwise, does not necessarily constitute or imply its endorsement, recommendation, or favoring by the United States Government or the University of California. The views and opinions of authors expressed herein do not necessarily state or reflect those of the United States Government or the University of California, and shall not be used for advertising or product endorsement purposes.

# Detection and classification of off-normal images during automatic alignment of high energy laser beams

James V. Candy, Wilbert A. McClay III, Abdul A. S. Awwal, S. Walter Ferguson  
and Scott C. Burkhart

University of California, Lawrence Livermore National Laboratory, P.O. Box 808, L-156, Livermore, CA 94526

Received March 1, 2005

High-energy laser beams, when focused appropriately, provide the potential for fusion reactions. However, when unfocused, they provide the potential for critical failure of the underlying systems and possible damage to expensive optical components. The fusion experiments at the Lawrence Livermore National Laboratory (LLNL), National Ignition Facility (NIF) have but one major purpose from the optical engineering viewpoint: to accurately focus 192 high energy laser beams on a nanoscale (mm) fusion target at the precise location and time. With this achieved, the fusion reaction will occur providing a major breakthrough in physics and the boundless applications. This paper is aimed at pre-processing alignment images to detect and classify any that cannot be precisely positioned in order to achieve ignition. We term these images “off-normal” because of their inherent ambiguities that could lead to misalignment and potential damage.

OCIS codes: 070.6020, 140.3300, 120.1880, 040.1520

## I. INTRODUCTION

The alignment of large operative, short pulse, laser systems is a significant and costly endeavor dating back to the early seventies.<sup>1</sup> Beam alignment is a complex and critical process requiring precise and accurate measurements. If beam alignment is not performed in an optimal manner, costly optics could be damaged disrupting an entire experiment. Early alignment systems proved inadequate due to inherent uncertainties and lack of reliability. Therefore, contemporary imaging systems evolved based on using video cameras to image and align the beam.<sup>1-10</sup> This approach estimates the current beam position from the image, adjusts mirrors relative to an accurate reference measurement of physical beam center and attempts to minimize the deviation between them.<sup>2-10</sup> Current systems employ the same basic principle, but utilize much improved high-resolution video cameras and more accurate position control systems.<sup>10</sup> However, even with these improved systems, should an anomalous or equivalently “off-normal” image occur due to component malfunctions (sticky mirror, stepping motor failure, component failure, etc.), the current system will still attempt to perform its alignment function unless there is some method to detect, classify and reject the erroneous image prior to position imaging and eventual control loop adjustments. This paper is concerned not only with detecting and classifying off-normal images, prior to processing, but also rejecting any anomalous images during laser system operations---without causing a major time disruption of the operations during these costly experiments. In this paper, we present a suite of operations under the above-mentioned constraints to detect, classify and reject any off-normal images prior to processing, thereby, enabling a minimal distortion of pulsed laser operations. This idea of pre-processing raw “off-normal” image data for position and detection is novel for large, pulsed laser systems.

High power, tightly focused laser beams are required to achieve successful ignition and therefore fusion at the Lawrence Livermore National Laboratory (LLNL) National Ignition Facility (NIF).<sup>11</sup> The beams simultaneously focus precisely on a nanoscale target capsule to succeed. Therefore, there are a large number of alignment measurements that must be performed along the NIF beam lines to assure that the pointing and alignment control system centers the beam in order to provide the maximum energy on the fusion target located in the associated chamber.<sup>11-13</sup> An automatic alignment (AA) system was designed and implemented to assure successful deployment of the high energy beam in each of the 192 beam lines. Initially, only four beam lines were constructed and aligned manually by well-trained operators and sophisticated diagnostic tools; however, a fully automated system is close to completion. Hence, the requirement of an “off-normal” detection implementation scheme is crucial. Each of the reference and measured beam images fall into different classes as will be observed and therefore a multitude of approaches must be undertaken to provide a timely detection, classification and rejection (if necessary) so another set of acceptable images can be generated, if the defect is not physical in nature. Therefore, there is a need for a pre-processing technique, which accepts as input uncertain reference and measurement images and performs the ultimate screening for alignment.

Before we launch into the details of the approach and algorithms, let us briefly describe the operation of the alignment procedure to emphasize the importance of the screening. The alignment images are acquired from a charge-coupled device (CCD) imaging camera producing both noisy reference and measurement images. The precise reference image is used to provide the desired fiducial that is used by the alignment system. Corrections to align the measured image with the reference is accomplished by using the dedicated control loops that adjust pointing mirror stepping motors until the deviations between both reference and measured positions are within acceptable limits.<sup>13</sup> Ultimately, the goal is to make this deviation zero assuring proper beam alignment. Thus, the smaller the XY-deviations, the closer the beam is to the centerline reference assuring a tightly focused, high energy beam on target---the goal of the alignment system.

The ideal approach to perform the detection, classification and off-normal rejection system is based on a very simple concept: “reduce the dense pixel image to a simple or set of simple functions that capture the essential features of the alignment pattern or inherent structure. In this sense, we are essentially attempting to define a two-dimensional to one-dimensional transformation ( $2D \rightarrow 1D$ ), while preserving the critical properties or features of the image under investigation---quite a technical challenge. Along with such a transformation associated signal processing must also be performed to minimize the inherent artifacts that accompany such a data acquisition system and yet enable a reliable decision function.

We develop a variety of such transformations in Sec. 2 with the associated processing after we develop the basic classification background to understand one of the major approaches. In Sec. 3 a set of ideal ensemble averaged images are constructed, transformed and detected to demonstrate the various approaches and evaluate their performance. We apply the transformation and processing algorithms to actual off-

normal images in the next section evaluating their overall performance and finally summarize the results and discuss future work.

## II. IMAGE TRANSFORMATIONS FOR OFF-NORMAL DETECTION

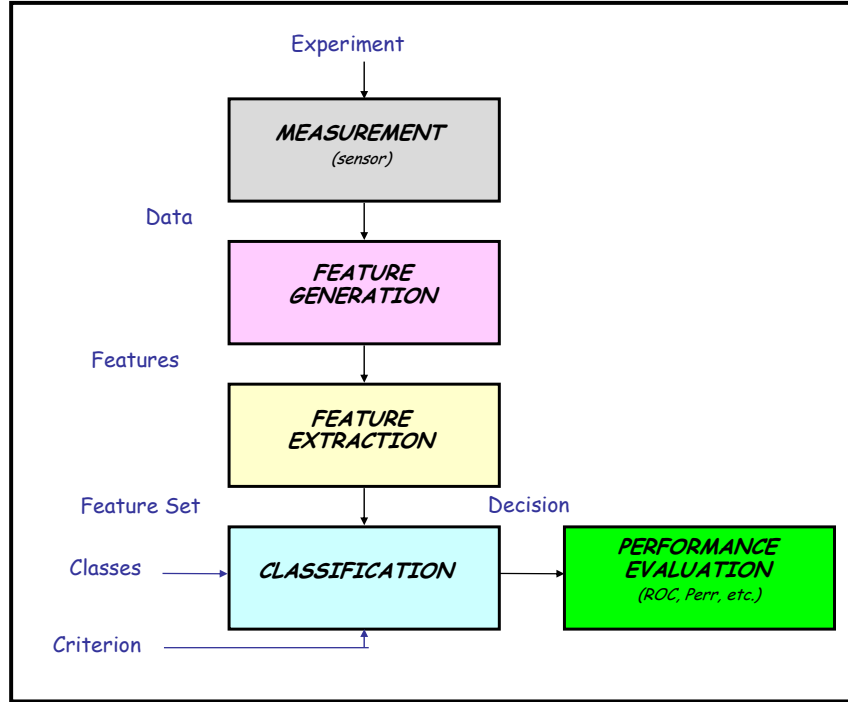
In this section we begin by examining some of the simpler alignment images to motivate our approach and then investigate the more technical. First, we consider the cases of black and white images, which actually are not as simple to diagnose as one might expect. Usually these images are created by faulty shutters, illumination, hardware failures etc. The approach that we take to design the processor is based on classification/detection theory. We decided to construct the *off-normal classifier/detector* as a two-stage processor: the first is a Bayesian-type classifier to determine the class the image belongs based on its unique probability mass function (PMF) features, while the second stage can be considered a feature detector based on tolerance parameters that must be satisfied for successful operation of the alignment system.<sup>14</sup>

The overall question that must be answered by the pre-processor is whether or not the incoming image is satisfactory (good) for further alignment processing or not satisfactory (bad). This is basically a decision problem, which can simply be restated as,

“GIVEN a noisy measured image, DETERMINE whether it is good or bad. IF good, pass it to the imaging alignment algorithm or IF bad, reject it.”

Once the decision is made, the image is processed accordingly. Unfortunately, there are a variety of images that fall into the bad class; therefore, we must define this class in more detail and develop a processor capable of performing the required decision. The basic idea is to find a set of unique characteristics of each “bad image” that can be used to make a reliable decision and reject it. This problem can then be handled as a classification problem. The main idea here is to determine the set of characteristics or features that uniquely capture the “badness” of an image enabling the classifier to “decide” that it is, in fact, bad and reject it.

A basic classifier structure is depicted in Fig. 1. Classifier development proceeds directly from the measurement data obtained from the CCD camera or from a set of simulated images. Once the image is acquired from the camera, the salient features are generated (e.g. mean, variance, etc.), then a feature subset is extracted. In the purest sense, all of the image pixels could be considered potential features; however, it is far better to select a reduced set in order to optimize classifier performance. The feature extraction is performed and provides the input for classification. In order to perform the classification, we define the classes (good or bad) and then select a criterion, which is used to make the decision. The performance of the classifier can be evaluated by a number of metrics that are meaningful to the underlying application. Some common methods are receiver operating characteristic (ROC) curve or equivalently the probability of error.



**Fig. 1.** Classification Development Structure: Data, Feature, Classifier and Performance.

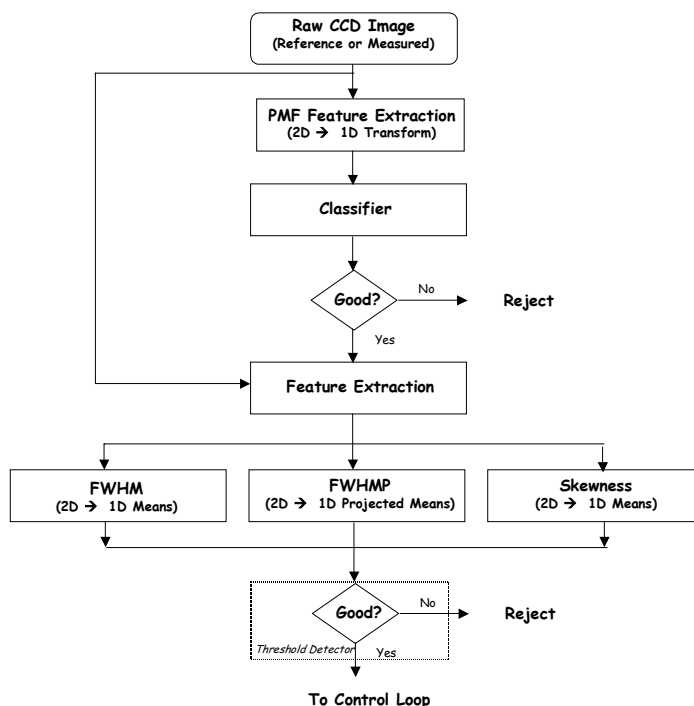
In this paper we will develop the concept of constructing a classifier/detector based on transforming the measured 2D image to generate meaningful 1D features. The basic structure is shown in Fig. 2 below. Once the raw NIF image data (reference or measured image) is captured by the CCD camera, it is transformed,  $2D \rightarrow 1D$  to generate a set of features that can be used for classification/detection. Because of the likelihood of the occurrence of black, white or noisy images, these are processed first. Should the image be accepted as “good”, it is passed on to a second set of detectors which again perform a variety of  $2D \rightarrow 1D$  transformations creating decision functions which can be tested against a prescribed threshold based on the characteristics of the expected image. Should the image be passed again, it is sent to the actual imaging algorithm for eventual position estimation (e.g. centroiding).

First, we choose to use the probability mass function as a means of generating our desired feature sets for the black and white problem. Once they are generated then the next step is to extract a subset of the features to be used for overall classification of incoming image.

#### A. Classification Approach

Classification is actually a special form of multiple hypothesis decision theory.<sup>14</sup> A classifier is essentially a rule to sort the features and assign them to a particular class. That is, it is an algorithm whose function is to separate the measurement or observation

space containing the features into regions that correspond to classes. Classification has its own particular jargon that we began to introduce in the previous section. To be more precise, we define the components of the processor. We start with the data,  $I(x,y)$ , which represents our measured NIF image (reference or alignment). From the data we generate a set of features that uniquely characterize the particular image. We can represent a number of features by the vector,  $\mathbf{f} \in \mathbb{R}^{N_f \times 1}$  for our problem. Recall that a feature is a subset of the measured data image that is used for classification. Feature selection is a methodology to select the salient features characterizing the particular data image. We choose to transform the image to a probability mass function using a histogram estimator in the first stage. From the histogram we then extract the features. Once extracted, they are processed by a classifier. For our processor we choose to use a *Bayesian-type classifier*.<sup>14</sup> This processor is based on designing a classifier capable of minimizing the classification error (probability). Next we discuss the development of an approximate Bayesian classifier and then apply it to our problem.



**Fig. 2.** NIF Off-Normal Image Classification/Detection: Classification and Detection Stages.

### 1. Bayesian Classification

Suppose we have  $N_c$ -classes of images and we would like to “decide” in which class,  $C_i$ , the current image,  $I(x,y)$  belongs. We define the posterior probability (after image is available) as  $\Pr(C_i | I(x,y))$ . This is essentially the information we are seeking

since it is the probability of the class,  $C_i$ , given the data (image)---exactly what is necessary to make our decision (good or bad). Using Bayes' rule<sup>14-17</sup>, we see that the posterior can be calculated using other more easily obtainable information, that is,

$$\Pr(C_i | I(x, y)) = \frac{\Pr(I(x, y) | C_i) \Pr(C_i)}{\Pr(I(x, y))} \quad (1)$$

where we define the likelihood as  $\Pr(I | C_i)$ , the prior probability as  $\Pr(C_i)$  and the evidence,  $\Pr(I)$ . So we can think of Bayes' rule as a transformation of the prior information through the likelihood to provide us with the desired estimate of the posterior probability, which will be used in the classifier.

In this formulation, we are obtaining the solution to the question that: Given the measured data (image), what is the probability that it belongs to class  $C_i$ ? Similarly, the question of: how likely is this class is measured by the likelihood in Bayes' rule? The prior is information (probability) we have available that can be used to distinguish one class from another before we have any measured data available. Here the question becomes: what prior information do we have about the class  $C_i$ ? Finally, the evidence is essentially a "scale" factor that is used to assure that the posterior is a true probability. In this formulation the data can be replaced by the features, since they are simply a transformation of the measured data into unique characteristics to describe the image and eventually classify it. Therefore we can rewrite Bayes' rule of Eq. (1) in terms of the feature vector as

$$\Pr(C_i | \mathbf{f}) = \frac{\Pr(\mathbf{f} | C_i) \Pr(C_i)}{\Pr(\mathbf{f})} \quad (2)$$

for  $\mathbf{f}$  defined as the  $N_f$ -dimensional feature vector. This equation forms the basis of our classifier.

The Bayesian classifier (general) for the multi-class ( $N_c$  classes), multi-feature ( $N_f$  features) problem is simply given by the relations

$$\Pr(C_i | \mathbf{f}) > \Pr(C_j | \mathbf{f}) \quad \forall i \neq j \quad (3)$$

that is, the decision is made based on which class has the maximum posterior probability. Expanding this expression over the  $N_c$ -classes gives

$$IF \rightarrow \begin{cases} \Pr(C_i | \mathbf{f}) > \Pr(C_1 | \mathbf{f}) \\ \Pr(C_i | \mathbf{f}) > \Pr(C_2 | \mathbf{f}) \\ \vdots \\ \Pr(C_i | \mathbf{f}) > \Pr(C_{N_c} | \mathbf{f}) \end{cases} \quad \text{CHOOSE } C_i \quad (4)$$



which states that if the posterior probability of class  $C_i$  is greater than the other class probabilities then “decide” that it is the true class of the image captured by its feature vector.

## 2. Bayesian Classifier Performance

Associated with this decision is the probability of error (making the wrong decision) given by

$$\Pr(\varepsilon) = \sum_{j=1}^{N_c} \Pr(\mathbf{f} | C_j) + \Pr(\mathbf{f} | C_i) \quad (5)$$

which means that we penalize the decision when we choose class  $C_j$  when the true class is  $C_i$  or visa-versa. Another method of estimating the performance is to use the probability of correct decision,  $\Pr(C_{\text{cor}})$ . This is preferred because there are fewer ways to make the right decision than wrong. This probability is defined by

$$\Pr(C_{\text{cor}}) := \sum_{j=1}^{N_c} \Pr(\mathbf{f} | C_j) \quad (6)$$

The error probability is a key issue in classification, since it tells us how well the classifier is performing, that is, it provides a performance metric. Consider the two-class problem (good or bad). In this case the Bayesian classifier is given simply by

$$\text{IF } \begin{cases} \Pr(C_1 | \mathbf{f}) > \Pr(C_2 | \mathbf{f}) \\ \text{Otherwise} \end{cases} \quad \begin{matrix} \text{CHOOSE } C_1 \\ \text{CHOOSE } C_2 \end{matrix}$$

with (7)

$$\Pr(\varepsilon) = \min[\Pr(C_1 | \mathbf{f}), \Pr(C_2 | \mathbf{f})]$$

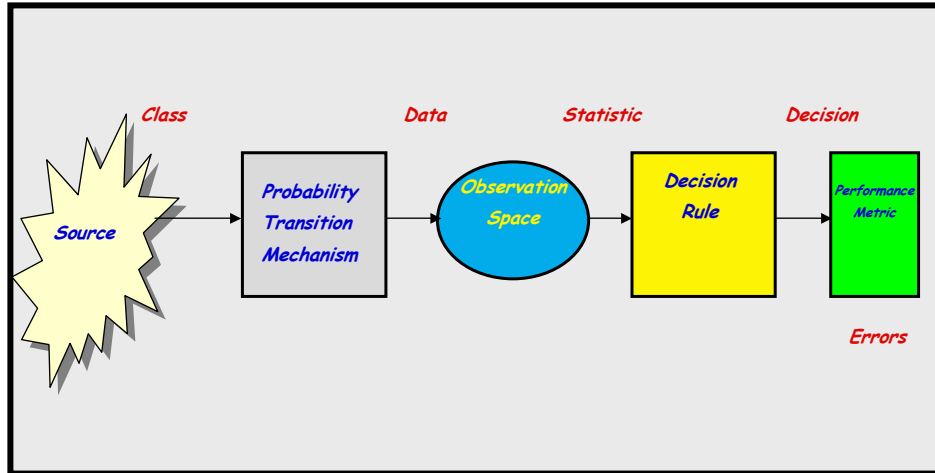
Thus, the Bayes’ classifier minimizes the probability of error or equivalently maximizes the probability of correct decision.

Suppose we divide the decision space into two regions: one corresponding to  $R_1$  and one to  $R_2$  here each region corresponds to classes  $C_1$  and  $C_2$ , respectively. Here there are two ways of making errors: choosing  $C_1$  when  $C_2$  is correct or visa-versa. Thus, the error probability is given by

$$\Pr(\varepsilon) = \Pr(\mathbf{f} \in R_2, C_1) + \Pr(\mathbf{f} \in R_1, C_2) = \Pr(\mathbf{f} \in R_2 | C_1) \Pr(C_1) + \Pr(\mathbf{f} \in R_1 | C_2) \Pr(C_2) \quad (8)$$

using Bayes' rule.

With this in mind we are now able to sketch the underlying foundation of the classification problem shown in Fig. 3. Here a source (laser beam) generates the class output from the beam line and through a probabilistic transition mechanism generating the data to be measured. The CCD camera images the beam. The resulting image is a point in the observation or measurement space where a decision rule (preprocessor) assigns each image to a class and a decision is made (good or bad). Finally the performance of the classifier is evaluated using the probability of error (or correct decision). This can be accomplished by Monte Carlo simulation methods or from a large database where we “know” the true class by generating an ensemble of realizations (images) and accumulating the error statistics to evaluate performance. This completes the sub-section on background, next we construct a classifier for our problem.



**Fig. 3.** Classification/Detection Problem: Source, Probability, Observation, Decision and Performance.

### 3. NIF Classifier Design

In this section we develop the classifier used as the part of the preprocessor for NIF alignment images. The approach follows the paradigm that the image is transformed to an estimate of a 1D PMF ( $2D \rightarrow 1D$ ). It is based on identifying and extracting a unique set of features for the most prevalent set of undesirable images (e.g. all black pixels). Thus, a unique features,  $\{f_k\}$ ,  $k=1, \dots, N_f$ , from selected off-normal images are

identified, extracted and classified. The features provide the direct input in a Bayesian-type classification scheme.

*a. Feature Generation*

Next we describe a transformation of the acquired image to another space for eventual feature extraction. One of the primary motivations for this approach is the need for real-time processing in this automatic alignment application. For our problem, we use the probabilistic features available in the estimated image intensity probability mass function,  $p(a)$ . For the estimator we use the histogram defined in terms of the intensity,  $a_n$ , such that

$$p(a = a_n) \approx \hat{H}(a_n) := \frac{N(a_n)}{N_T} \quad \text{for } n = 0, \dots, N_a - 1 \quad (9)$$

where  $N(a_n)$  is the number of occurrences of intensity  $a$  in the  $n^{\text{th}}$  bin (e.g.  $a_{255}$  is the counts in the 255-intensity bin) and  $N_T$  is the total number of intensities available in the image or the number of pixels,  $N_a$  is determined by the number of bits available, that is, for our 8-bit images,  $N_a = 2^{N_{\text{bits}}} = 256$  intensity values ranging from 0 to 255. For a given interval, say  $[a_{n-1}, a_n]$ , we have that

$$N_T = \sum_{n=0}^{N_a-1} N(a_n) \quad (10)$$

with  $a_0$  the number of zero-intensity counts. An example histogram is shown in Fig. 4 defining these terms. The histogram is an estimate of the PMF, which can be used to estimate the probability of intensity values

$$\Pr(a) = \sum_n p(a = a_n) = \sum_n \hat{H}(a_n) \quad \text{for all } n \text{ such that } a_n \leq a \quad (11)$$

Clearly, if we desire the probability of the intensity taking on values in a given range, then using the histogram estimate, we have

$$\Pr(a_i \leq a \leq a_j) = \sum_{n=i}^j p(a_i \leq a \leq a_j) = \sum_{n=i}^j \hat{H}(a_n) \quad (12)$$

In essence, our data, the measured images has been transformed to a 1D-estimate of the PMF using the histogram. Next we must extract a set of features from the PMF that uniquely characterize common (bad) images we expect to encounter in our data sets.

b. *Feature Extraction*

We define the components of the feature vector,  $\mathbf{f}$ , by a set of probabilities that will uniquely characterize an image by a class. Currently, we are considering four major classes: white, black or noise<sup>♦</sup>, that is,

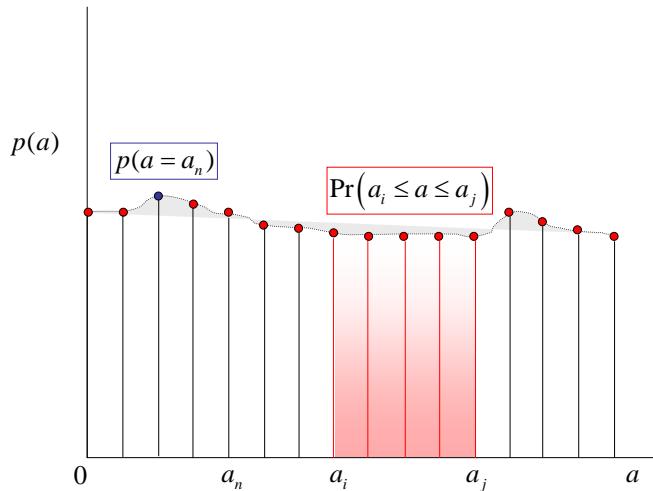
$$C := \{C_1, C_2, C_3, C_4\} \text{ for } C_1 \rightarrow \text{White}; \text{ for } C_2 \rightarrow \text{Black}; \text{ for } C_3 \rightarrow \text{Noise}; \text{ for } C_4 \rightarrow \text{Valid Image} \quad (13)$$

Our images are modeled in terms of the features of their corresponding intensities, that is,

$$I(x, y) = \{a_n\}; \quad a_i < a_n < a_j, \quad n = 1, \dots, N_a \quad (14)$$

where the pixilated image is  $I(x, y)$  for  $x = 1, \dots, N_x; y = 1, \dots, N_y$  with set of intensities,  $\{a_n\}$  bound by the prescribed interval  $[a_i, a_j]$ . Corresponding to this definition, we can define the probability that the intensity of the  $k^{\text{th}}$ -feature will occur in this interval as

$$\Pr(a_i < a < a_j) = p_k \quad (15)$$



**Fig. 4.** Probability Mass Function for Image Intensities.

<sup>♦</sup> We use seven (7) classes in the actual classifier, since there are four types of *black* images we must consider in the NIF problem.

We define this probability as a component of our feature vector, estimated by the histogram for each particular image that will be used in the classifier, that is,

$$f_k = \hat{p}_k = \sum_{n=i}^j \hat{H}(a_n) \quad (16)$$

where  $f_k$  is the  $k^{\text{th}}$ -component of the feature vector estimated by summing the histogram over the interval,  $[a_i, a_j]$ . The classifier is then constructed as discussed in the previous section based on the conditional probability of the feature vector,  $\Pr(\mathbf{f} | C_\ell)$ .

For our problem using an 8-bit image, we must define the various types of images that can occur in our NIF beam line and characterize or model them by their features in terms of the probability intervals. We start with the various classes of *black* images, since these represent the most prevalent type and are of high concern.

Black images are more difficult to characterize, since there are varieties of the image that must be accounted for in the feature vector. For instance, an “all black” or pure black image is simple in that all of its pixel intensities are zero, that is,

$$I(x, y) = 0 \quad \forall a_n; \quad \text{with } f_1 = \hat{p}_1 = \hat{H}(0) \quad \text{[PURE BLACK]} \quad (17)$$

Another type of black image we frequently encounter is called a “good black” image that is the most typical of the black class and is defined by

$$I(x, y) = a_n \quad \ni \quad 17 < a_n < 19 \quad \text{with } f_2 = \hat{p}_2 = \sum_{n=17}^{19} \hat{H}(a_n) \geq \tau_{\text{prob}} \quad \text{[GOOD BLACK]} \quad (18)$$

where  $\tau_{\text{prob}}$  is a probability bound of expected performance (e.g. 0.98) for good classification.

On the other hand, a “bad black” image is one that should not occur imply a potential physical problem with the CCD camera. It is defined by

$$I(x, y) = a_n \quad \ni \quad 1 < a_n < 9 \quad \text{with } f_3 = \hat{p}_3 = \sum_{n=0}^9 \hat{H}(a_n) \geq \tau_{\text{prob}} \quad \text{[BAD BLACK]} \quad (19)$$

A “normal black” image is characterized by

$$I(x, y) = a_n \quad \ni \quad 10 < a_n < 26 \quad \text{with } f_4 = \hat{p}_4 = \sum_{n=10}^{26} \hat{H}(a_n) \geq \tau_{\text{prob}} \quad \text{[NORMAL BLACK]} \quad (20)$$

A white image is defined by the property that its intensity is given by

$$I(x, y) = a_n \quad \ni \quad 225 < a_n < 255 \quad \text{with} \quad f_5 = \hat{p}_5 = \sum_{n=225}^{255} \hat{H}(a_n) \quad \text{[WHITE]} \quad (21)$$

which means that the white image intensities range from [225,255] and its feature (probability) is estimated by summing the estimated image intensity histogram over the defined range.

The next image that we define is a “noise image” characterized by its low probability over the entire intensity band. Since the noise is essentially equally likely in each pixel, one approach to model it is to assume its probability is low relative to the other images. In this case we have found from our data base that

$$I(x, y) = a_n \quad \ni \quad 0 < a_n < 255 \quad \text{with} \quad f_6 = \hat{p}_6 = \hat{H}(a_n) < \mathbf{0.2} \quad \text{[NOISE]} \quad (22)$$

Typical images that have fiducials created by alignment masks must also be classified and passed on to the pre-processor for off-normal condition detection. We call these images “valid” or “good” for further processing. This feature is defined by

$$I(x, y) = a_n \quad 0 < a_n < 255 \quad \text{with} \quad f_7 = \hat{p}_7 = 1 - \sum_{k=1}^6 \hat{p}_k \geq \tau_{\text{prob}} \quad \text{[GOOD]} \quad (23)$$

Thus, with these models for each of the image types, we create a feature vector,  $\mathbf{f} \in R^{7 \times 1}$  and construct the Bayesian-type classifier of the previous section, that is, we estimate each of the individual class probabilities from the given features,  $\Pr(C_\ell | \mathbf{f})$ , and then select the largest over all classes (blacks, white, noise, good) to determine the true class

$$\max \Pr(C_\ell | \mathbf{f}) \quad \text{for} \quad \ell = 1, \dots, 7 \quad (24)$$

### CLASSIFIER ALGORITHM

1. Transform the image to the 1D histogram function;
2. Estimate the feature vector component for each expected type of “off-normal” image specified above from Eqs. (21)-(23);
3. Choose the class (blacks, white, noise, good) based on the  $\max \Pr(C_\ell | \mathbf{f})$ .

This completes the classifier-based, off-normal detector, next we investigate other features of more typical images assuming they have not been rejected by this detector using the above algorithm.

#### 4. *Feature Detection Techniques*

In this section we develop procedures that are performed *after* the Bayesian-type classification has been performed to screen out the typical off-normal images. Here we actually have an image with the potential alignment mask (e.g. 2D gaussian pulse), but it could be distorted for a number of reasons discussed in the introduction. Thus, we have a valid image but it may possess “undesirable” features that would cause the alignment algorithm to give poor position estimate to the control loop. Our approach is the same, 2D  $\rightarrow$  1D image transformation, but now we exploit properties of the beam quality that have been specified during the beam line design. From experience, we can allow a more liberal tolerance than the actual design specifications to perform the detection enabling a more robust performance of the detector.

##### a. *Full Width Half Maximum (FWHM) Detector*

In this sub-section we discuss the development of the FWHM off-normal detection technique, which proves to be very robust over our main laser beam lines. Again the major idea follows by transforming the image to two 1D functions, the row mean,  $\bar{I}_x$ , and the column mean,  $\bar{I}_y$ , defined by

$$\bar{I}_x(y) := \sum_{j=1}^{N_x} I(x_j, y_k); k = 1, \dots, N_y \text{ for } \bar{I}_x \in \mathbb{R}^{N_y \times 1} \quad (25)$$

$$\bar{I}_y(x) := \sum_{j=1}^{N_y} I(x_j, y_k); j = 1, \dots, N_x \text{ for } \bar{I}_y \in \mathbb{R}^{N_x \times 1}$$

Typically, these averages take the form of a pulse, either wide or narrow, depending on the 2D structure (e.g. 2D gaussian image  $\rightarrow$  1D gaussian pulses); therefore, we define FWHM in the usual manner, that is,

$$I_{FWHM}(y) := \frac{1}{2} \bar{I}_x(y) \Big|_{y=y_n; y=y_m} \text{ for } y_n > y_m \quad (26)$$

$$I_{FWHM}(x) := \frac{1}{2} \bar{I}_y(x) \Big|_{x=x_n; x=x_m} \text{ for } x_n > x_m$$

From specifications for a given image, we know, a-priori, what the allowable interval or pulse width is for a given alignment loop. So we can define the respective allowable interval tolerances that are calculated from these values as

$$\Delta I_x(y) := I_{FWHM}(y_n) - I_{FWHM}(y_m) \leq \tau_x \quad (27)$$

$$\Delta I_y(x) := I_{FWHM}(x_n) - I_{FWHM}(x_m) \leq \tau_y$$

where  $\tau_x$  and  $\tau_y$  are specified by the specific alignment loop (e.g. FOA loop is 10 pixels). We also use a generalized form of the FWHM detector by performing multiple projections through the images at other angles as discussed next.

*b. Full Width Half Maximum (FWHMP) Projection Detector*

In this sub-section we discuss the development of the FWHMP off-normal detection technique, which can robustly handle the case where the 2D pulse shape is clipped at an angle. Again the major idea follows by transforming the image to two 1D functions, the angular row mean,  $\bar{I}_{x\theta}$ , and the angular column mean,  $\bar{I}_{y\theta}$  where  $\theta$  is the projection angle. In our case we limit the angle to the set,  $\{0^\circ, 45^\circ, 90^\circ, 135^\circ\}$  where the  $0^\circ$  and  $90^\circ$  cases are precisely,  $\bar{I}_{y0}(x) = \bar{I}_y(x)$  and  $\bar{I}_{x90}(y) \equiv \bar{I}_x(y)$ . In essence, we are only calculating two additional angular means, which are equivalent to calculating line integrals at particular projection angle similar to straight-line projection tomography.<sup>18</sup>

*c. Skewness Detector*

In this sub-section we discuss the development of a skewness detector based on processing the projection data. Even though skewness is a statistical measure of central tendency, it can be used to provide us with useful pulse shape information. In statistics the skewness is based on the locations of the mean, median and mode of the test distribution. For our problem, if we consider our pulse to be that of a gaussian-like distribution, then it is a simple calculation to indicate any abnormalities in its projected shape. Skewness of a perfectly symmetrical (distribution) pulse is “0” with its (mean, median, mode centrally located). If the pulse shape is non-symmetrical and lopsided to the left, then it is positively skewed, “+”, while if lopsided to the left it is negatively skewed or “-“. If the 2D (gaussian-like) pulse is clipped at an angle its projection will be weighted to the right or left; therefore, it can be detected by the skewness statistic is calculated by<sup>15</sup>



$$S_x(y) = \frac{E\left\{\left(\bar{I}_x(y) - \mu_y\right)^3\right\}}{\sigma_y^3} \quad \text{for } \mu_y = \sum_{k=1}^{N_y} \bar{I}_x(y_k) \quad \text{and} \quad \sigma_y = \sqrt{\sum_{k=1}^{N_y} \left(\bar{I}_x(y_k) - \mu_y\right)^2} \quad (28)$$

$$S_y(x) = \frac{E\left\{\left(\bar{I}_y(x) - \mu_x\right)^3\right\}}{\sigma_x^3} \quad \text{for } \mu_x = \sum_{j=1}^{N_x} \bar{I}_y(x_j) \quad \text{and} \quad \sigma_x = \sqrt{\sum_{j=1}^{N_x} \left(\bar{I}_y(x_j) - \mu_x\right)^2}$$

The actual process is to locate the actual maximum of the average (e.g. gaussian pulse) and cut a window of  $\pm 50$  samples on either side of the maximum minimizing the noise in the skewness window. The skewness statistic is then calculated on the windowed pulse.

#### *d. Pre-Processing*

Many of the images have a varying intensity (bright-to-dim or dim-to-bright) depending on its illumination. This variation creates a trend in the projection data means; therefore, we remove it with a linear trend fit that is performed quite simply by locating the two endpoints of the 1D projection, creating the trend from the standard linear equation (slope is  $\Delta y / \Delta x$ , intercept is  $b$ ). Typically, we actually define the endpoint 25 pixels in from the true endpoint to avoid any end effects created by the projection operation. Trend removal need not be perfect for the detection, since we only require the maximum location of the projection result.

This completes the discussion of the pre-processor used for off-normal detection, next we apply it to synthesized and actual measured images.

### **III. OFF-NORMAL DETECTION PERFORMANCE ON ENSEMBLE IMAGES**

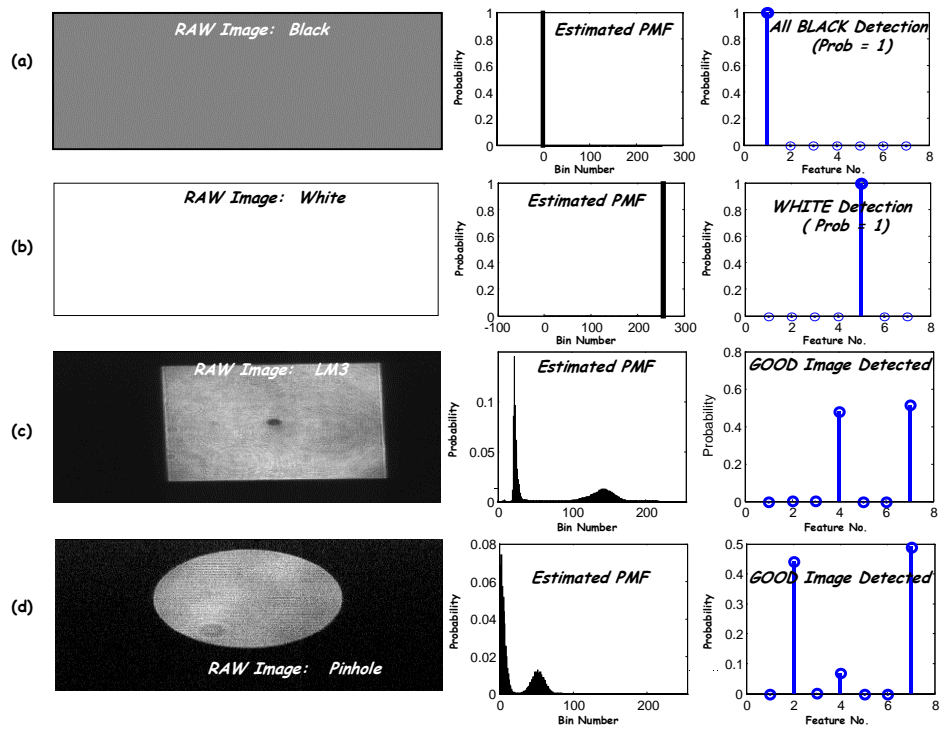
In this section, we discuss the application of the off-normal suite of 1D detection algorithms and demonstrate their performance on ensemble averaged off-normal images, that is, the test images are generated by a result of averaging an ensemble ( $> 30$  members) of an alignment loop CCD camera output.

#### *A. Classifier Performance*

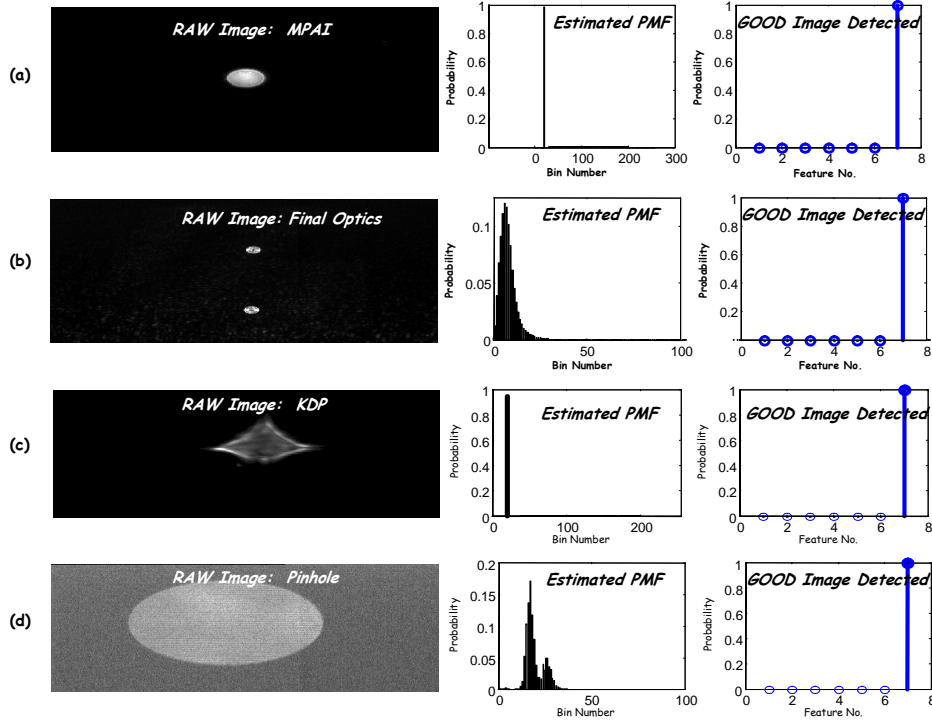
In this sub-section we investigate the performance of the classifier on a set of images to characterize its performance. A typical set of classifier outputs are shown in Fig. 5. We see in 5a and 5b that both the raw pure black and white images are easily detected and classified by their unique features. Note from the histogram estimates and feature probabilities,  $\Pr(f_n | C_\ell)$ , validate the classifications. In Fig. 5c and 5d we observe the linear mirror output, LM3, image as well as a small pinhole (gaussian-like

pulse) in beam center and the large pinhole alignment image. These figures demonstrate strong normal black ( $f_4$ ) and good ( $f_7$ ) values, but in both cases the “good” feature is maximum and selected by the classifier.

After a number of runs, it was found that quite a number of valid or “good” images that could be processed were not selected by the classifier because of the large number of black pixels populating the image (e.g. small pinhole image) as illustrated in Fig 6a (MPAI) and 6b (Final Optics) images. We modified the feature selection by incorporating another constraint that sets its probability to zero if the probability threshold constraint is not satisfied. Compare the classifier outputs in Figs. 5 and 6. The effect of this approach demonstrated that it was possible to even correctly classify the black (or white) dominant images robustly as well. The results are clearly demonstrated in Fig. 6a-d. Note the black dominated KDP and Pinhole images are correctly classified by including this additional feature constraint. The classifier was also executed over an ensemble of 1000 all black images and was able to perform with less than 5% classification error (detection probability of  $>0.95$ ) that is acceptable for this application because the subsequent off-normal tests are able to detect and reject the “bad” images.



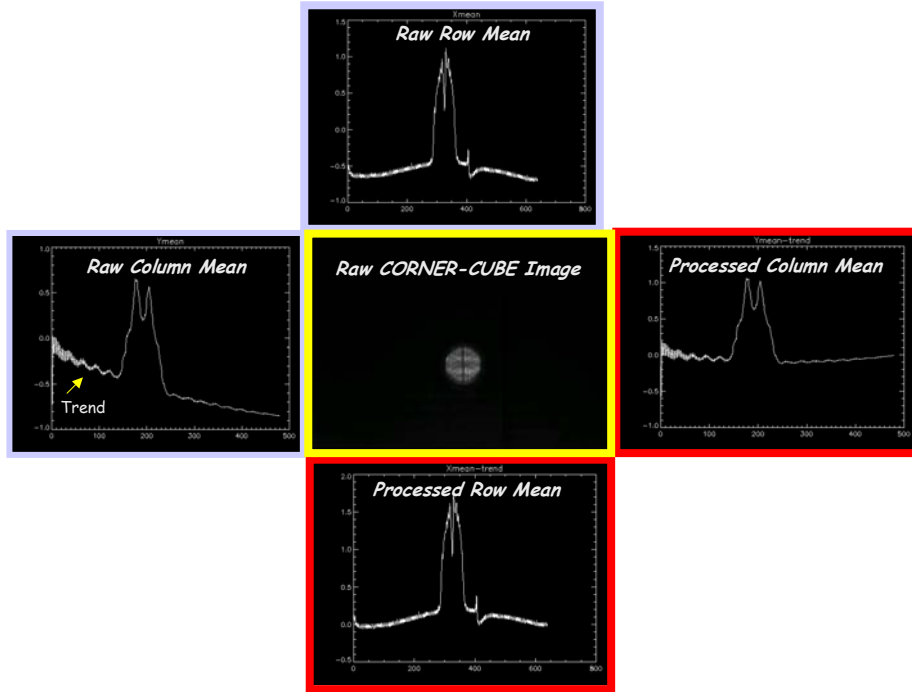
**Fig. 5.** Classifier outputs for: (a) Pure black image. (b) Pure white image. (c) LM3 image. (d) Pinhole image.



**Fig. 6.** Classifier outputs for: (a) MPAI image. (b) Final optics image. (c) KDP image. (d) Pinhole image.

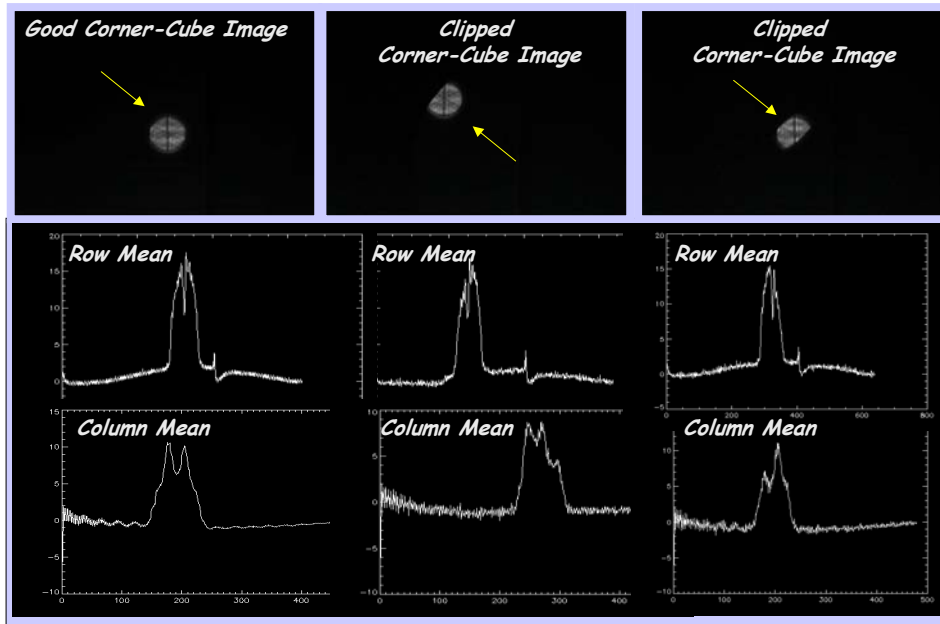
### B. Back-Lit Corner-Cube Reflection Images

The back-lit corner-cube reflection image is used in many beam lines to perform the alignment and eventual beam position estimation. A typical raw image (center box) is shown in Fig. 7 with the corresponding raw and processed row and column means. The image was acquired from the actual NIF beam line during “diagnostic” firing of the alignment laser. It consists of the ensemble average of 30-60 “shots” or firings. In this case, the beam was aligned with the reference successfully. The column mean has a distinguishable trend that is removed as part of the processing, while the row mean has a DC-offset that is also removed. The FWHM test was performed on these 1D functions indicating that the image was satisfactory for further processing.



**Fig. 7.** Raw Corner-Cube Back Reflection Image and FWHM (2D  $\rightarrow$  1D) Detection after pre-processing (trend removal).

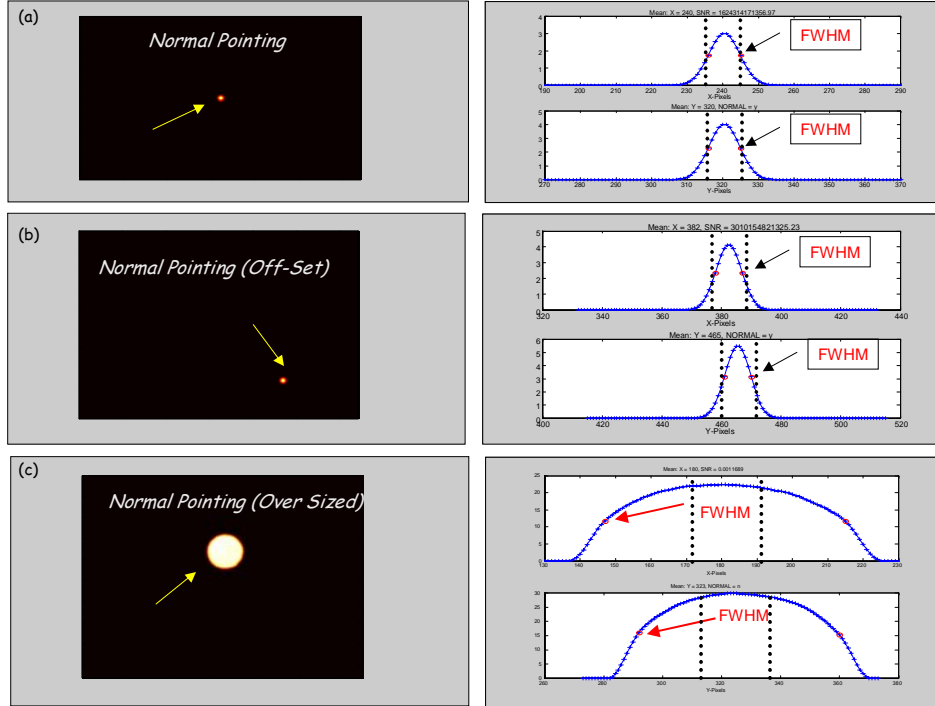
Next we investigate the case of off-normal, corner-cube algorithms that are processed in much the same manner using the FWHM and skewness tests to detect any anomalies.<sup>19-21</sup> The results for the “good” and “bad” images are shown in Fig. 8 where we see the raw images in the upper row followed by the column and row means after preprocessing. The first image was satisfactory and passed the FWHM and skewness tests while the other “clipped” images were rejected. Here the combined test was sufficient to reject these bad images. However, it was discovered that even if these tests were passed it was possible to still have bad images pass. This led to the development of the FWHMP that incorporates these tests including the additional  $45^\circ$  and  $135^\circ$  projections capable of robustly detecting this class of off-normal imaging.



**Fig. 8.** Corner-Cube FWHM/Skewness Testing: Good and Clipped Images (pass, reject, reject).

### C. Pinhole Images

Perhaps the simplest and most frequently used alignment algorithm is termed normal pointing and it is used in over 20 of the 34 control loops for either the reference or measured image position estimates. This algorithm is applied to the pinhole images shown in Fig. 9 for position estimation. However, we first perform the FWHM diagnostic and specifications for a “good” image for off-normal detection. The pre-processing consisted of trend removal and averaging to perform the  $2D \rightarrow 1D$  transformation using the row and column means and the FWHM test as depicted in the figure. In Fig. 9a we observe an almost perfect gaussian-like pulse and the resulting row and column mean signal extracted from the image---this image was accepted and passed on to the algorithm for position estimation. The same type of result is shown in Fig. 9b. Although this image is off-set to the lower right, it can still be easily aligned by the position estimation algorithm; therefore, it is also passed, since it satisfies the FWHM specification test shown by the vertical lines. An off-normal image is shown in Fig. 9c and the performance of the FWHM clearly detects its condition and rejects the image. Thus, we see the robust performance of this processor on ideal (ensemble averaged) pinhole images.



**Fig. 9.** Pinhole Images from NIF Beam line: (a) Ideal pinhole image ensemble average. (b) Ideal pinhole image ensemble average with off-set. (c) Oversized pinhole image ensemble average (off-normal) rejected.

This completes the section on the performance of the off-normal classification/detection algorithm suites with application to ensemble averaged images (reduced noise), next we apply the approach to actual noisy images and evaluate their overall performance.

#### IV. OFF-NORMAL CLASSIFICATION/DETECTOR RESULTS

In this section we discuss the application of the off-normal classifier/detector to a set of test images. The results are depicted in the subsequent tables that demonstrate its performance.

We discuss two typical alignment loops. The first loop alignment using back lit corner cube pinhole images. Table I describes the summarized results from a set of backlit-corner-cube-pinhole images that could be obtained during the operation of this loop caused by some opto-mechanical malfunction. Nominal images are shown in image numbers 1 and 8. They are circular with six diametrically placed lines at equi-angular positions. The last column of Tables I and II show whether an image *passes* as normal

image by the off-normal preprocessor (termed *PP*). It also shows whether the algorithm is able to process the image as a normal image.

The criterion is based on a *tolerance threshold*,  $T$ ,

$$|L(\theta) - \mu_L| \leq T \quad (29)$$

for  $L(\theta)$  the width (in pixels) of a line at angle,  $\theta$ , which could be  $0^\circ$ ,  $45^\circ$ ,  $90^\circ$  or  $135^\circ$  and  $\mu_L$  is the expected line width. Note that all four measurements along  $0^\circ$ ,  $45^\circ$ ,  $90^\circ$ ,  $135^\circ$  must be within  $T=20$  pixels of the expected width, otherwise it will be rejected by the preprocessor (*PP*).

Image number 1 is obtained by averaging 30 nominal images. The typical diameter of the image should be 78 pixels. However, since all the pinholes are situated on a single wheel, it is possible to have a different pinhole in the path, The second and third images are examples of such off-normal condition. These cases are rejected by the above criterion.

Another type of off-normal could result when the image of the pinhole is obstructed by the presence of a circular aperture in the path limiting its field of view. Image numbers, 4 and 5 shows such examples. The X-FWHM and Y-FWHM widths together is not able to detect these cases. There are cases of image 4, where X-FWHM and Y-FWHM widths are calculated as 62 pixels, which are within 20 pixels of the expected size and accepted as a normal image. This prompted us to add the additional testing at 45 and 135 angles. Note that 135 angle was able to generate a condition favorable for rejection of both images 4 and 5.

It should also be pointed out that the back-lit corner-cube image is produced by two light sources superimposing the corner cube image to a common point. Ideally, the pointing direction is such that both sources produce images that appear to be a single image. When their pointing direction is not properly aligned, it is possible to have the two views of the corner cube image completely separate from each other as shown in images 6 and 7 of Table I. Note that both of these cases produce a high Y-FWHM width value and are rejected.




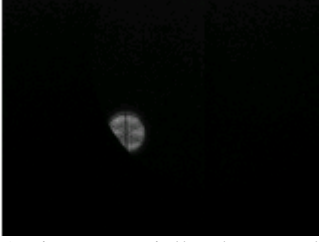
The nominal image in number 8 should be accepted, although it exhibits prominent diffraction effects resulting in fringes overlapped with the corner cube image. Note however, it affects the Y-FWHM width and hence shows a lower value. It passes through the off-normal detector and is processed by the algorithm. Note that images 3-6 are all processed by the algorithms, since they all have one valid image and produces a center value. However, the off-normal detector flags an uncertainty value of 640, which automatically shuts down the alignment loop. It forces the control operators to examine the image before letting the automatic alignment process continue. Thus with this arrangement of producing of high uncertainty given by the off-normal detector, the risk of mechanical failure is highly minimized.





Table II lists a normal pinhole image from another alignment loop in the NIF laser system. Note that the first two cases are pinholes of larger radii. The expected diameter is same as the last case, 78 pixels. The first two images fail based on the FWHM criterion. The third image results from superposition of light from a secondary light source known as the ISP source. This case is rejected based on the X-FWHM and Y-FWHM width. The images 4 and 5 both pass the preprocessor. Note that the lowest dimension of 60 pixels is within 20 pixels of the expected dimension. Changing the threshold to less than 18 will declare a failure for this image. If from NIF beam operation, it becomes a necessity to reject this condition, then it can be excluded by modifying the rejection threshold criterion. The double image is rejected due to high Y-FWHM width. Next four cases are some typical background images that are rejected by the off-normal detector as zero or black image. The other two cases show that they are also rejected by the FWHM width criterion.

This completes the illustration of the performance of the off-normal classifier/detector. Its performance over out alignment image suites has been outstanding as demonstrated by these runs.








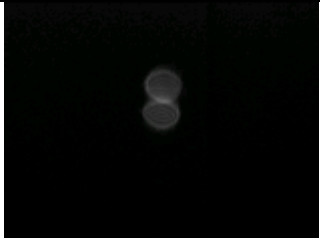
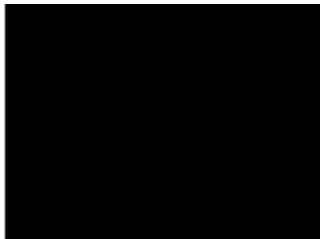


**TABLE I. NIF CONTROL LOOP No. 1 OFF-NORMAL DETECTOR PERFORMANCE.**


Number	Image Loop Name	Detection Statistics	Result
1.	 Nominal (averaged) image	Xskew, Yskew -(1.00818, -0.736816)  Skew_45 = -0.974718 Skew_135 = -0.982363  X-FWHM WIDTH 75 Y-FWHM WIDTH 79  Crosswidth_1 73.5391 Crosswidth_2 73.5391  Expected_Size 78	<b><u>PASS</u></b> (PP,ALG)
2.	 A 150 micro-radian pinhole	Xskew, Yskew -(0.964835, -0.906968)  Skew_45 = -2.04531 Skew_135 = -1.67676  X-FWHM width = 217 Y-FWHM width = 214  Crosswidth_1 = 183.848 Crosswidth_2 = 188.090  Expected_Size = 78	<b><u>FAIL</u></b> (PP)
3.	 A 200 micro-radian pinhole	Xskew, Yskew - (0.996913, -0.911543)  Skew_45 = -2.00253 Skew_135 = -1.23729  X-FWHM width = 290 Y-FWHM width = 285  Crosswidth_45 = 210.72 Crosswidth_135 = 210.7  Expected_Size = 78	<b><u>FAIL</u></b> (PP,ALG)
4.	 An image partially obstructed by the aperture	X_cut_skew -0.878841 Y_cut_skew 0.716805  X-FWHM WIDTH 62 Y-FWHM WIDTH 62  Crosswidth_45 = 70.7 Crosswidth_135 = 55.15  Expected_Size 78	<b><u>FAIL</u></b> (PP,ALG)

5.	 <p>A pinhole image obstructed by two mirrors</p>	Skewness in X: -1.7207 Skewness in Y: -.1989  X-FWHM WIDTH 63 Y-FWHM WIDTH 53  Crosswidth_45 = 67.88 Crosswidth_135 = 48.08  Expected_Size 78	<b><u>FAIL</u></b> (PP) Process(ALG)
6.	 <p>A double image produced by change in pointing direction of the two incident beams</p>	Skewness in X: 0.1924 Skewness in Y: 0.83627  X-FWHM WIDTH 69 Y-FWHM WIDTH 115 Crosswidth_45 = 89.1 Crosswidth_135 = 101.8 Expected_Size 78	<b><u>FAIL</u></b> (PP) Process(ALG)
7.	 <p>A double image produced by change in pointing direction of the two incident beams</p>	Skewness in X: 0.260571 Skewness in Y: 0.358135  X-FWHM WIDTH 67 Y-FWHM WIDTH 211  Crosswidth_45 = 115.97 Crosswidth_135 = 158.4  Expected_Size 78	<b><u>FAIL</u></b> (PP) Process(ALG)
8.	 <p>A nominal image</p>	Xskew,Yskew - (0.594575, 0.0195767)  X-FWHM WIDTH 71 Y-FWHM WIDTH 61  Crosswidth_45 67.88 Crosswidth_135 69.3  Expected_Size 78	<b><u>PASS</u></b> (PP,ALG)

**TABLE II. NIF CONTROL No. 2 LOOP OFF-NORMAL DETECTOR PERFORMANCE.**

Number	Image Loop Name	Detection Statistics	Result
1.	 <p>150 micron pinhole image</p>	Xskew, Yskew $-(0.636380, -1.60995)$ Skew_45 = $-0.828526$ Skew_135 = $-1.87832$ X-FWHM WIDTH 195 Y-FWHM WIDTH 209 Crosswidth_1 197.990 Crosswidth_2 192.333 Expected_Size 78	<b>FAIL</b> (PP,ALG)
2.	 <p>200 micron pinhole image</p>	Xskew, Yskew $-(0.581036, -1.21950)$ Skew_45 = $-1.35347$ Skew_135 = $-1.72134$ X-FWHM WIDTH 270 Y-FWHM WIDTH 271 Crosswidth_1 168.291 Crosswidth_2 152.735 Expected_Size 78	<b>FAIL</b> (PP,ALG)
3.	 <p>CSF image with a ISP far field light sources accidentally turned on</p>	Xskew, Yskew $-(0.250812, -0.234559)$ Skew_45 = $-1.15389$ Skew_135 = $-1.05802$ X-FWHM WIDTH 60 Y-FWHM WIDTH 53 Crosswidth_1 60.8112 Crosswidth_2 67.8822 Expected_Size 78	<b>FAIL</b> (PP) Process(ALG)
4.	 <p>A nominal pinhole image corresponding to a 50 micron pinhole produced two properly aligned light sources called LM1 LM3 passing through a single pinhole</p>	Xskew, Yskew $-(0.815371, -0.828966)$ Skew_45 = $-0.858294$ Skew_135 = $-0.832382$ X-FWHM WIDTH 70 Y-FWHM WIDTH 67 Crosswidth_1 66.4680 Crosswidth_2 69.2965 Expected_Size 78	<b>PASS</b> (PP,ALG)

5.	 <p>A nominal distorted pinhole by misaligned light sources</p>	<p>Xskew, Yskew <math>-(0.930212, -0.992664)</math></p> <p>Skew_45 = <math>-0.91140</math> Skew_135 = <math>-1.48225</math></p> <p>X-FWHM WIDTH 70 Y-FWHM WIDTH 60</p> <p>Crosswidth_1 62.2254 Crosswidth_2 66.4680</p> <p>Expected_Size 78</p>	<p><b>PASS</b> (PP) Process(ALG)</p>
6.	 <p>Double pinhole caused by pointing mismatch of the two LM1_LM3 light sources</p>	<p>Xskew, Yskew <math>-(1.11357, -0.0796157)</math></p> <p>Skew_45 = <math>0.318868</math> Skew_135 = <math>0.721725</math></p> <p>X-FWHM WIDTH 69 Y-FWHM WIDTH 108</p> <p>Crosswidth_1 80.6102 Crosswidth_2 90.5097</p> <p>Expected_Size 78</p>	<p><b>FAIL</b> (PP) Process(ALG)</p>
7.	 <p>A background image with all zeros</p>	<p>IMAGE STANDARD DEVIATION 0.0000000</p> <p>*** PURE BLACK Image Detected ***</p>	<p><b>FAIL</b> (PP,ALG)</p>
8.	 <p>A background with higher camera gain</p>	<p>X-FWHM WIDTH 0 Y-FWHM WIDTH 475</p> <p>*** NOISE Black Image Detected ***</p>	<p><b>FAIL</b> (PP,ALG)</p>
9.	 <p>Background from the csf pinhole loop with few bad pixels</p>	<p>X-FWHM WIDTH 389 Y-FWHM WIDTH 475</p> <p>*** NOISE Black Image Detected ***</p>	<p><b>FAIL</b> (PP,ALG)</p>

10.	 <p data-bbox="354 430 667 451">Background from ISP camera</p>	<p data-bbox="743 193 1211 220">IMAGE STANDARD DEVIATION</p> <p data-bbox="743 220 1211 247">1.4958835</p> <p data-bbox="743 247 1211 275">0.899170</p> <p data-bbox="743 310 1211 338">*** NORMAL Black Image Detected ***</p>	<p data-bbox="1230 193 1416 220"><b>FAIL</b> (PP,ALG)</p>
-----	---	---	---

## V. SUMMARY

We have developed an off-normal (image) classifier/detector based on the concept of transforming the original two-dimensional image to a one-dimensional function and extracting a variety of features that uniquely characterize each of the off-normal conditions. We developed a two-stage classifier/detector based on Bayesian classification principles. The design does not strictly adhere to the Bayesian formalism, since the appropriate conditional probabilities have not been estimated. However, the concept of features and their underlying probabilities have been exploited to develop an ad-hoc classification scheme coupled with a set of detection algorithms to determine off-normal images and inhibit their eventual processing. The performance of the classifier/detector has been investigated with great success on various ensembles of test images from the NIF data base. A 95% detection probability was achieved on the class of black images. We conclude from our processing that the classifier/detector is capable of correctly detecting off-normal images with high probability in this hostile environment.

## ACKNOWLEDGMENT

We appreciate the technical advice and guidance from Dr. Erlan Bliss and Karl Wilhelmsen of LLNL NIF Program during this study. This work was performed under the auspices of the U. S. Department of Energy by University of California, Lawrence Livermore National Laboratory under Contract No. W-7405-Eng-48.

## CORRESPONDING AUTHOR

James V. Candy, University of California, Lawrence Livermore National Laboratory,  
P.O. Box 808, L-156, Livermore, CA 94526  
Phone: 925-422-8675  
Email: [candy1@llnl.gov](mailto:candy1@llnl.gov)

## REFERENCES

1. D. Speck, E. Bliss, J. Glaze, J. Herris, F. Holloway, J. Hun, B. Johnson, D. Kuizenga, R. Ozarski, H. Patton, P. Ruppert, G. Suski, C. Swift and C. Thompson, "The Shiva laser-fusion facility," *IEEE J. Quantum Electr.*, Vol. QE-17, No. 9, pp. 1599-1619, (1981).
2. J. Liu, H. Furuhashi, A. Torii, R. Sharma, V. Chitnis, B. Singh, J. Yamada, and Y. Uchida, "Automatic mask alignment in the theta direction using moiré sensors," *Nanotechnology*, **6**, pp. 135-138, (1995).
3. W. Blum, H. Kroha, P. Widmann, "A novel laser-alignment system for tracking detectors using transparent silicon strip sensors," *IEEE Trans. Nuclear Sci.*, Vol. 43, No. 3, 1194-1199, (1996).
4. G. Seward, J. Leszcynski and E. Mulhern, "Rapid alignment of laser beams within optical systems," *Opt. Eng.*, **36** (5), pp. 1414-1420, (1997).
5. A. Adolph, A. Boscheron, A. Dulac and E. Journot, "Final optics design for the megajoule laser," *SPIE Proceedings*, Vol. 3492, pt. 1-2, pp.44-50, (1999).
6. W. He, Q. Chen, R. Xu, Z. Peng, H. Yang, C. Zhu, and J. Zhao, "Image transfer based automatic alignment technique for laser-fusion facility," *Acta Optica Sinica*, Vol. 19, No. 9, pp. 1279-1283, (1999).
7. S. Roth, S. Schael, and G. Schmidt, "A test of the laser alignment system ALMY at the TTF-FEL," *Nuclear Instr. Methods Phys. Res. A*, Vol. 475, pp 537-544, (2001).
8. N. Fleurot, A. Adolf, M. Andre, J. Bruneau, C. Cavailler, M. Novaro, P. Philippe, F. Kovacs, B. Le Garrec, J. Di Nicola and J. Leidinger, "The ligne d'integration laser (LIL): construction status and first 1-w early results," *Proc. SPIE*, Vol. 4948, pp. 418-424, (2003).
9. D. Liu, J. Zhu, R. Zhu, D. Fan, "Laser beam automatic alignment in multipass amplifier," *Opt. Eng.*, **43** (9), pp. 2066-2070, (2004).
10. R. Zacharias, N. Beer, E. S. Bliss, S. Burkhart, S. Cohen, S. Button, R. Van Atta, S. Winters, J. Salmon, M. Latta, C. Stoiz, D. Pigg and T. Arnold, "Alignment and wavefront control systems of the National Ignition Facility," *Opt. Eng.*, **43** (12), pp. 2873-2884, (2004).
11. E. Moses, "The National Ignition Facility Comes to Life," *Science & Technology Review*, Lawrence Livermore National Lab. Report, pp. 4-14, Sept. (2003).
12. F. R. Holderner, E. Ables, E. S. Bliss, S. J. Boege, R. D. Boyd, C. J. Choccol, D. T. Davis, R. D. Demaret, R. E. English, C. W. Laumann, J. L. Miller and S. W. Thomas, "Beam control and diagnostic functions in the NIF transport spatial filter," *Proceedings of SPIE 3047*, Ed. Michel Andre, 692-699, (1996).
13. E. S. Bliss, F. R. Holderner, J. T. Salmon, J. R. Severyn, et. al., "Beam control and laser diagnostic systems," Lawrence Livermore National Lab. Report, UCRL-LR-105821-99-1, 79-97, (1999).
14. R. O. Duda, P. E. hart and D. G. Stork, *Pattern Classification*, (John Wiley, New York, 2001).
15. R. L. Winkler and W. L. Hays, *Statistics: Probability, Inference and Decision*, (Holt, Rinehart and Winston, New York, 1975).
16. T. W. Anderson, *An Introduction to Multivariate Statistical Analysis*, (John

- Wiley, New York, 1984).
17. A. Papoulis, *Probability, Random Variables, and Stochastic Processes*, (McGraw-Hill, New York, 1965)
  18. K. R. Castleman, *Digital Image Processing*, (Prentice-Hall, Englewood Cliffs, 1979).
  19. A. Awwal, W. McClay, W. Ferguson, J. Candy, T. Salmon and P. Wegner, "Composite amplitude modulated phase-only filter based detection and tracking of the back-reflection of KDP images," in *Photonic Devices and Algorithms for Computing VI*, Eds. K. Iftekharuddin and A. A. S. Awwal, Proc. of SPIE **5556**, (2004).
  20. M. A. Karim and A. A. S. Awwal, *Optical Computing: An Introduction*, John Wiley, New York, NY, 1992.
  21. J. V. Candy, W. A. McClay III, A. A. S. Awwal, and W. Ferguson, "Optimal Centroid position estimation," in *Photonic Devices and Algorithms for Computing VI*, edited by K. Iftekharuddin and A. A. S. Awwal, Proc. of SPIE 5556 (SPIE Bellingham, WA, 2004), pp. 249-260.